Available online at www.sciencedirect.com

ScienceDirect

Ceramics International 37 (2011) 1459–1463

CERAMICS INTERNATIONAL

www.elsevier.com/locate/ceramint

Preparation and characterization of CeO_2/TiO_2 nanoparticles by flame spray pyrolysis

Choowong Chaisuk [a], Anusara Wehatoranawee [a], Sirichai Preampiyawat [a], Sirirat Netiphat [a], Artiwan Shotipruk [b], Joongjai Panpranot [b], Banjerd Jongsomjit [b], Okorn Mekasuwandumrong [a,*]

[a] *Department of Chemical Engineering, Faculty of Engineering and Industrial Technology, Silpakorn University, Nakorn Pathom 73000, Thailand*

[b] *Center of Excellence on Catalysis and Catalytic Reaction Engineering, Department of Chemical Engineering, Faculty of Engineering, Chulalongkorn University, Bangkok 10330, Thailand*

Received 28 May 2010; received in revised form 19 September 2010; accepted 3 November 2010

Available online 2 December 2010

Abstract

Nanocrystalline TiO_2, CeO_2 and CeO_2-doped TiO_2 have been successfully prepared by one-step flame spray pyrolysis (FSP). Resulting powders were characterized with X-ray diffraction (XRD), N_2-physisorption, Transmission Electron Microscopy (TEM) and UV–Vis spectrophotometry. The TiO_2 and CeO_2-doped TiO_2 nanopowders were composed of single-crystalline spherical particles with as-prepared primary particle size of 10–13 nm for Ce doping concentrations of 5–50 at%, while square-shape particles with average size around 9 nm were only observed from flame-made CeO_2. The adsorption edge of resulting powder was shifted from 388 to 467 nm as the Ce content increased from 0 to 30 at% and there was an optimal Ce content in association with the maximum absorbance. This effect is due to the insertion of $Ce^{3+/4+}$ in the TiO_2 matrix, which generated an n-type impurity band.

Keywords: Flame spray pyrolysis; CeO_2/TiO_2; Nanoparticles; Band-gap

1. Introduction

Titanium dioxide (TiO_2) has attracted strong attention due to its outstanding mechanical, thermal, electrical and photocatalytic properties. It has found appeal to many potential applications including a semiconductor in dye-sensitized solar cell [1], water and air treatment materials [2,3], photocatalytic splitting of water for green-energy hydrogen fuel [4,5] and catalysts and catalyst supports [6]. Its performance in these applications depends on its physical and chemical properties which are related to synthetic conditions. In order to improve the properties of TiO_2, many research groups attempted to modify TiO_2 visible wavelength by doping by elements [7,8].

Cerium oxide (CeO_2) is rare-earth oxide material used in the fields of photoluminescence, photosensitive material and anti-UV radiation. It has attracted large attention in catalysis due to its ability to store/release oxygen as an oxygen reservoir via the redox shift between Ce^{4+} and Ce^{3+} under oxidizing and reducing conditions. Improvement of photocatalytic activity by addition of Ce atoms in TiO_2 has already been reported [9–11]. The CeO_2–TiO_2 nanopowders have not been used in the photocatalyst field but also in the other catalytic applications [12].

Many techniques have been applied for preparing of TiO_2, CeO_2 and CeO_2–TiO_2 powders like; chemical vapor deposition [13], precipitation [14], magnetron sputtering [15], hydrothermal synthesis [16], sol gel synthesis [17], and spray pyrolysis [18]. Flame synthesis is a commercial process to make nanoparticles in large quantity and low cost [19,20]. Flame spray pyrolysis (FSP) is a technique that is capable of producing a wide variety of product compositions, which can be used such sensors [21], catalysts and catalyst supports [22–24]. TiO_2 and CeO_2 have already been made by FSP with close control of particle size, morphology, and crystallinity [25,26]. Here we report a possibility of rapid, flame synthesis of TiO_2, CeO_2 and CeO_2–TiO_2 powders with characterization of their morphology, particle size and UV absorption with increasing Ce content.

* Corresponding author.
E-mail address: okornm@yahoo.com (O. Mekasuwandumrong).

0272-8842/$36.00
doi:10.1016/j.ceramint.2010.11.018

2. Experimental

2.1. Powder synthesis

Precursor solutions were prepared by dissolving appropriate amounts of titanium (IV) butoxide ($Ti(OC_4H_9)4$, 97% Aldrich) and ammonium cerium (IV) nitrate ($(NH_4)_2Ce(NO_3)_6$, 99.99% Aldrich) in anhydrous ethanol (C_2H_5OH, T.J.). The metal concentration was kept constant at 0.3 M. The Ce contents were varied from 5 to 100 at%.

Nanocrystalline TiO_2, CeO_2 and CeO_2–TiO_2 powders were synthesized using flame spray pyrolysis (FSP) technique. In a typical run of the flame spray reactor, the liquid precursor mixture was fed into the center of a methane/oxygen flame by a syringe pump (at precursor feed rate of 5 ml/min in this experiment) and dispersed by oxygen (Thai Industrial Gas Co., Ltd.), to forming the fine spray. At the nozzle, the pressure drop at the capillary tip was kept constant at 1.5 bar by adjusting the orifice gap area. The spray flame was ignited by a smaller flame ring issuing from an annular gap. This premixed methane/oxygen (Thai Industrial Gas Co., Ltd.) supporting flame was kept constant with flow rate of 4.5 L/min and fuel/oxygen ratio of 1.5/3 L methane/L oxygen. A sintered metal plate ring (8 mm wide, starting at a radius of 8 mm) provided an additional oxygen sheath flow (5 L/min) surrounding the supporting flame. Particle products were collected on a glass microfibre filter (Whatman) with the aid of a vacuum pump.

2.2. Powder characterization

X-ray diffraction (XRD) patterns were recorded with a Siemens D5000 using nickel filtered Cu Kα radiation. The crystallite size (d_{XRD}) was determined using the Scherrer equation and α-alumina as the external standard. The rutile content was calculated from diffraction peak by using the equation as shown below:

$$W_R = \left[1 + 0.8\frac{I_A}{I_R}\right]^{-1} \quad (1)$$

where I_A and I_R represented integrated intensities of anatase and rutile diffraction peak, respectively. The BET surface area, average pore size diameters, and pore size distribution are determined by physisorption of nitrogen (N_2) using a BEL-SORP automated system. The morphology and particle size of powders were observed using a JEOL-JEM 200CX transmission electron microscope. The UV–Vis absorption spectra and band gap energy of nanopowders were obtained by using Lambda 650 UV/Vis spectrophotometer to study in electronic properties. The spectrophotometer was scanned around wavelength of 200–900 nm and obtained by UV WinLab software from Perkin-Elmer. The estimated band gap energy from the absorption spectra for catalysts were found by extrapolation the energy intercept of a plot of $(\alpha h\nu)^{1/2}$ versus $h\nu$ yield E_i for the allowed indirect transition ($n = 2$ from the follow equation)

$$\alpha = \frac{B(h\nu - E_g)^n}{h\nu} \quad (2)$$

where B is constant, E_g the optical band gap, α the absorption coefficient, $h\nu$ the photon energy, and n is an index. XPS experiments were carried out at National Synchrotron Research Center, using a VG Scientific α110 energy analyzer with Al Kα (1486.6 eV). The excitation scan of 400 W, analyzer voltage of 2.6 kV and the pass energy of the analyzer was 50 eV. Peak assignments were calculated using Thermo Avantage software and all spectra are referenced to an adventitious C 1s binding energy of 285.0 eV.

3. Results and discussion

Fig. 1 shows the XRD patterns of the flame-made TiO_2, CeO_2 and CeO_2–TiO_2 powder. Flame-made TiO_2 powder exhibited the characteristic peaks of anatase titania with some contamination of rutile phase and flame-made CeO_2 shows a typical diffraction pattern of cubic fluorite CeO_2. In the CeO_2–TiO_2 mixed oxides, the anatase phase contents decreased with increasing of Ce content and transformed completely after Ce loading was 30 at%. Additional peaks of cubic CeO_2 were also observed at Ce contents of 5 at% and higher. The diffraction peaks due to cubic fluorite CeO_2 in CeO_2–TiO_2 mixed oxides appear with the increasing concentration of CeO_2 for 5 at% of Ce.

TEM images of all powders are presented in Fig. 2. The flame-made TiO_2 powders consist of predominately spherical particles with the size around 10–20 nm with a low degree of aggregation. Adding 5–30 at% of Ce had no effect on the particle shape and aggregation state. The square-shape particles with average size around 8.2 nm were observed for pure flame-made CeO_2.

Table 1 summarizes the physiochemical properties of all FSP-made powder. Rutile contents increased from 17 to 77% as the Ce contents increased from 0 to 10 at% and then only rutile phase was observed after the Ce loading was higher than 30 at%. The crystallite size of anatase phase decreased from 17 to 14 nm as increasing Ce content from 0 to 10 at%. In a similar way, the crystallite size of rutile phase decreased from 18 to

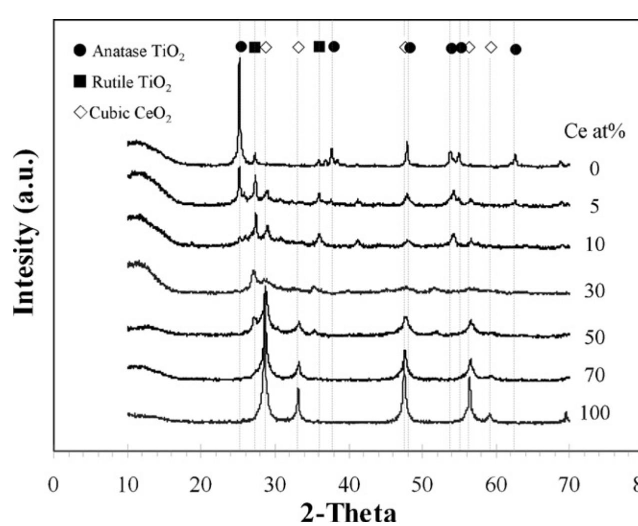

Fig. 1. XRD patterns of the FSP-derived TiO_2, CeO_2 and CeO_2–TiO_2 powders.

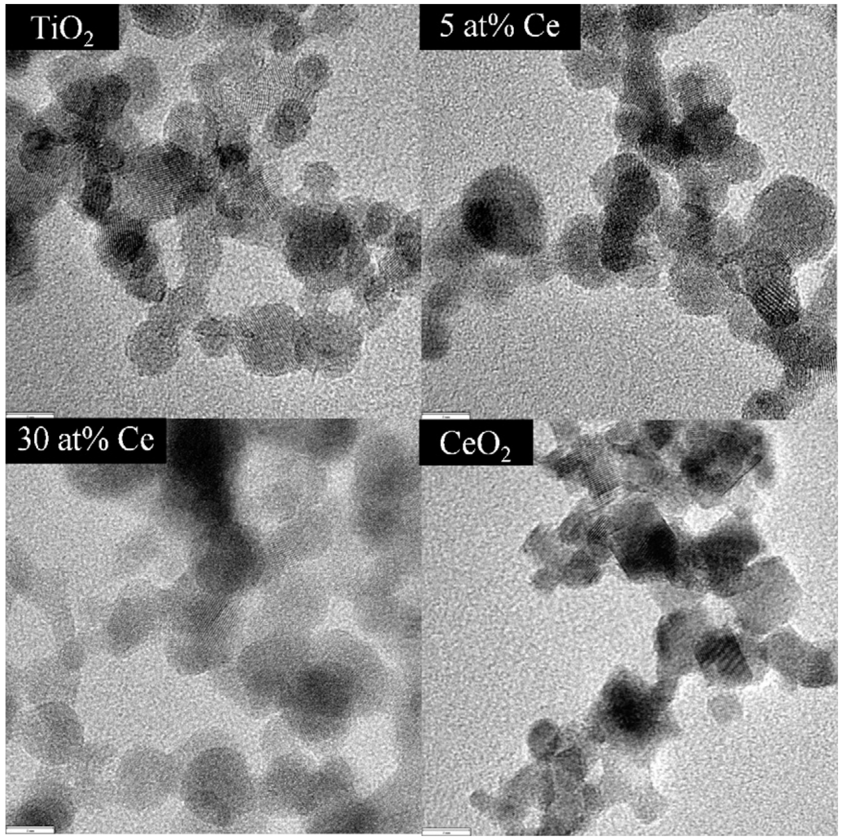

Fig. 2. TEM micrographs of the FSP-derived TiO_2, CeO_2 and CeO_2–TiO_2 powders.

7 nm as the increase in Ce content from 0 to 30 at%. The effect of decreasing of TiO_2 crystallite size and increasing of rutile contents after additions of second elements was also found in FSP-made Cu/TiO_2 and Fe/TiO_2 [27,28]. The authors proposed that doping by second element creates a higher number of defects, most likely oxygen vacancies, inside the TiO_2 crystal, thus accelerating the anatase to rutile transition and retard the crystallite growth. In our experiment, the specific surface area of powder decreased from 82.5 to 34.8 m^2/g with Ce doping from 0 to 30 at% and next for pure CeO_2, BET surface area increased to 77.3 m^2/g.

Normally, the addition of Ce in TiO_2 retards the anatase–rutile phase transformation. It can be explained by the introducing of cerium ions into TiO_2 which produces some deformation of the lattice structure and additional deformation energy, followed by which retards the transition from anatase to rutile phase [17,29–31]. However, in this work, addition of Ce atom accelerates the rutile phase transformation. This would be explained by the different preparation routes. In literatures, Ce modified TiO_2 particles were normally prepared via wet chemical routes, while the particle formation in FSP process occurred at high temperature at short residence time coupled with high quenching rate in gas phase [32]. Formation of nanoparticles by FSP was considered as follows: the sprayed droplets of precursor solution were evaporated and combusted as soon as they met the flame and released the metal atoms, then nucleation and growth of particles by coagulation and condensation occurred along the axial direction of the flame.

UV–visible spectra of pure TiO_2, CeO_2, and CeO_2–TiO_2 nanoparticles are shown in Fig. 3. The absorption edge, λ° for all catalysts ranged between 467 and 388 nm. The adsorption at 388 nm is characteristic of TiO_2 and the CeO_2–TiO_2

Table 1
The physiochemical properties of FSP-made powders.

Catalysts	Crystal phase	Anatase:rutile ratio	BET surface area (m^2/g)	Crystallite size		
				Anatase (nm)	Rutile (nm)	CeO_2 (nm)
TiO_2	Anatase–Rutile	17	82.5	17	18	n/a
5 at% CeO_2–TiO_2	Anatase–Rutile	53	76.6	15	16	n/a
10 at% CeO_2–TiO_2	Anatase–Rutile	77	74.5	14	9	n/a
30 at% CeO_2–TiO_2	Rutile–CeO_2	100	34.8	n/a	7	5.5
50 at% CeO_2–TiO_2	Rutile–CeO_2	100	54.3	n/a	7	10
70 at% CeO_2–TiO_2	Rutile–CeO_2	100	72.8	n/a	n/a	12
CeO_2	CeO_2	–	77.3	n/a	n/a	7

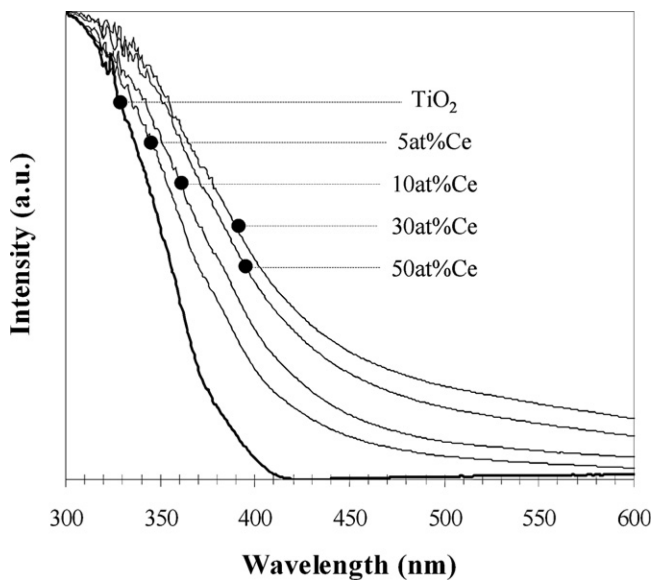

Fig. 3. UV–visible spectra of pure FSP-derived TiO_2, CeO_2, and CeO_2–TiO_2 powders.

nanopowder shifted the adsorption band toward to visible range (300–800 nm). The adsorption edges of pure TiO_2, 3 at% CeO_2–TiO_2, 5 at% CeO_2–TiO_2, 10 at% CeO_2–TiO_2, and 30 at% CeO_2–TiO_2 were extended to about 388, 418, 420, 435, and 467 nm, respectively. The absorbance variation increases with increase of cerium content up to 30 at%. For higher Ce contents, the absorbance decrease. Red shifts of flame-made CeO_2–TiO_2 would be attributed to the charge-transfer between the impurity band and the conduction band of TiO_2 [17]. This would occurred by the replacement of Ti^{4+} ions by $Ce^{4+/3+}$ sites to form an interfacial phases, which could be deemed and formed impurity band of interfacial with n-type identity. Moreover, the absorbance of the rare earth metal-doped sample was found to increase with increasing rare earth content. This suggest that the solid solution between CeO_2 and TiO_2 can be formed by using FSP technique and the maximum Ce loading amount by this method is 30 at%.

4. Conclusion

Nanocrystalline TiO_2, CeO_2 and CeO_2-doped TiO_2 have been successfully prepared by one-step flame spray pyrolysis (FSP). Resulting TiO_2 and CeO_2-doped TiO_2 nanopowders were composed of single-crystalline spherical particles with as-prepared primary particle size of 10–13 nm for Ce doping concentrations of 5–50 at%. While the square-shape particles with average size around 8.2 nm were only observed in flame-made CeO_2. The adsorption band of obtained powder was shifted to visible range (300–800 nm) as the Ce doping contents increased to 30 at%.

Acknowledgements

The authors would like to thank Thailand Research Fund (TRF) grant number DBG52 Bunjerd Jongsomjit for financial supports of the project.

References

[1] B. O'Regan, M. Grätzel, A low-cost, high-efficiency solar cell based on dye-sensitized colloidal TiO_2 films, Nature 353 (1991) 737–740.
[2] J.A. Byrne, B.R. Eggins, N.M.D. Brown, B. McKinney, M. Rouse, Immobilisation of TiO_2 powder for the treatment of polluted water, Applied Catalysis B: Environmental 17 (1998) 25–36.
[3] P. Supphasrirongjaroen, P.W. Kongsuebchar, J. Panpranot, O. Mekasuwandumrong, C. Satayaprasert, P. Praserthdam, Dependence of quenching process on the photocatalytic activity of solvothermal-derived TiO_2 with various crystallite sizes, Industrial & Engineering Chemistry Research 47 (2008) 693–697.
[4] M. Ni, M.K.H. Leung, D.Y.C. Leung, K. Sumathy, A review and recent developments in photocatalytic water-splitting using TiO_2 for hydrogen production, Renewable & Sustainable Energy Reviews 11 (2007) 401–425.
[5] R. Abe, K. Sayama, K. Domen, H. Arakawa, A new type of water splitting system composed of two different TiO_2 photocatalysts (anatase, rutile) and a IO_3^-/I^- shuttle redox mediator, Chemical Physics Letters 344 (2001) 339–344.
[6] P. Weerachawanasak, O. Mekasuwandumrong, M. Arai, S.-I. Fujita, P. Praserthdam, J. Panpranot, Effect of strong metal-support interaction on the catalytic performance of Pd/TiO_2 in the liquid-phase semi-hydrogenation of phenylacetylene, Journal of Catalysis 262 (2009) 199–205.
[7] R. Asahi, T. Morikawa, T. Ohwaki, K. Aoki, Y. Taga, Visible-light photocatalysis in nitrogen-doped titanium oxides, Science 293 (2001) 269–271.
[8] T. Ohno, Preparation of visible light active S-doped TiO_2 photocatalysts and their photocatalytic activities, Water Science and Technology 49 (2004) 159–163.
[9] L.Q. Jing, X.J. Sun, W.M. Cai, X.Q. Li, H.G. Fu, H.G. Hou, N.Y. Fan, Photoluminescence of Ce doped TiO_2 nanoparticles and their photocatalytic activity, Acta Chimica Sinica 61 (2003) 1241–1245.
[10] A.M.T. Silva, C.G. Silva, G. Drazic, J.L. Faria, Ce-doped TiO_2 for photocatalytic degradation of chlorophenol, Catalysis Today 144 (2009) 13–18.
[11] X. Jingjing, A. Yanhui, F. Degang, A novel Ce, C-codoped TiO_2 nanoparticles and its photocatalytic activity under visible light, Applied Surface Science 256 (2009) 884–888.
[12] S. Yang, W. Zhu, J. Wang, Z. Chen, Catalytic wet air oxidation of phenol over CeO_2–TiO_2 catalyst in the batch reactor and the packed-bed reactor, Journal of Hazardous Materials 153 (2008) 1248–1253.
[13] U. Qureshi, C.W. Dunnill, I.P. Parkin, Nanoparticulate cerium dioxide and cerium dioxide–titanium dioxide composite thin films on glass by aerosol assisted chemical vapour deposition, Applied Surface Science 256 (2009) 852–856.
[14] V. Štengl, S. Bakardjieva, N. Murafa, Preparation and photocatalytic activity of rare earth doped TiO_2 nanoparticles, Materials Chemistry and Physics 114 (2009) 217–226.
[15] S.-F. Wang, Y.-F. Hsu, R.-L. Lee, Y.-S. Lee, Microstructural evolution and phase development of Nb and Y doped TiO_2 films prepared by RF magnetron sputtering, Applied Surface Science 229 (2004) 140–147.
[16] J.R. Xiao, T.Y. Peng, R. Li, Z.H. Peng, C.H. Yan, Preparation, phase transformation and photocatalytic activities of cerium-doped mesoporous titania nanoparticles, Journal of Solid State Chemistry 179 (2006) 1161–1170.
[17] Z.L. Liu, B. Guo, L. Hong, H.X. Jiang, Preparation and characterization of cerium oxide doped TiO_2 nanoparticles, Journal of Physics and Chemistry of Solids 66 (2005) 161–167.
[18] G.P. Fotou, S.E. Pratsinis, Photocatalytic destruction of phenol and salicylic acid with aerosol-made and commercial titania powders, Chemical Engineering Communication 151 (1996) 251–269.
[19] R. Strobel, A. Alfons, S.E. Pratsinis, Aerosol flame synthesis of catalysts, Advanced Powder Technology 17 (2006) 457–480.
[20] W.J. Stark, S.E. Pratsinis, Aerosol flame reactors for manufacture of nanoparticles, Powder Technology 126 (2002) 103–108.

[21] T. Sahm, L. Mädler, A. Gurlo, N. Barsan, S.E. Pratsinis, U. Weimar, Flame spray synthesis of tin dioxide nanoparticles for gas sensing, Sensors and Actuators B: Chemical 98 (2004) 148–153.

[22] S. Somboonthanakij, O. Mekasuwandumrong, J. Panpranot, T. Nimmanwudtipong, R. Strobel, S.E. Pratsinis, P. Praserthdam, Characteristics and catalytic properties of Pd/SiO_2 synthesized by one-step flame spray pyrolysis in liquid-phase hydrogenation of 1-heptyne, Catalysis Letter 119 (2007) 346–352.

[23] O. Mekasuwandumrong, S. Somboonthanakij, P. Praserthdam, J. Panpranot, Preparation of nano-Pd/SiO_2 by one-step flame spray pyrolysis and its hydrogenation activities: comparison to the conventional impregnation method, Industrial & Engineering Chemistry Research 48 (2009) 2819–2825.

[24] S. Pisduangdaw, J. Panpranot, C. Methastidsook, C. Chaisuk, K. Faungnawakij, P. Praserthdam, O. Mekasuwandumrong, Characteristics and catalytic properties of $Pt–Sn/Al_2O_3$ nanoparticles synthesized by one-Step flame spray pyrolysis in the dehydrogenation of propane, Applied Catalysis A: General 370 (2009) 1–6.

[25] W.Y. Teoh, L. Mädler, D. Beydoun, S.E. Pratsinis, R. Amal, Direct (one-step) synthesis of TiO_2 and Pt/TiO_2 nanoparticles for photocatalytic mineralisation of sucrose, Chemical Engineering Science 60 (2005) 5852–5861.

[26] L. Mädler, W.J. Stark, S.E. Pratsinis, Flame-made ceria nanoparticles, Journal of Material Research 17 (2002) 1356–1362.

[27] A. Teleki, N. Bjelobrk, S.E. Pratsinis, Flame-made Nb- and Cu-doped TiO_2 sensors for CO and ethanol, Sensors and Actuators B: Chemical 130 (2008) 449–457.

[28] W.Y. Teoh, R. Amal, L. Mädler, S.E. Pratsinis, Flame sprayed visible light-active $Fe–TiO_2$ for photomineralisation of oxalic acid, Catalysis Today 120 (2007) 203–213.

[29] Q.-Z. Yan, X.-T. Su, Z.-Y. Huang, C.-C. Ge, Sol–gel auto-igniting synthesis and structural property of cerium-doped titanium dioxide nanosized powders, Journal of the European Ceramic Society 26 (2006) 915–921.

[30] E. Borgarello, J. Kiwi, M. Gratzel, E. Pelizzetti, M. Visca, Visible light induced water cleavage in colloidal solutions of chromium-doped titanium dioxide particles, Journal of American Chemical Society 104 (1982) 2996.

[31] A.W. Xu, Y. Gao, H.Q. Liu, The preparation, characterization, and their photocatalytic activities of rare-earth-doped TiO_2 nanoparticles, Journal of Catalysis 207 (2002) 151.

[32] M.C. Heine, L. Mädler, R. Jossen, S.E. Pratsinis, Direct measurement of entrainment during nanoparticle synthesis in spray flames, Combustion and Flame 144 (2006) 809–820.